Numerical Simulation of Natural Convection in Annuli with Internal Fins

Man Yeong Ha*, Joo Goo Kim
School of Mechanical Engineering, Pusan National University, San 30, Chang Jeon Dong, Kuem Jeong Gu, Pusan 609-735, Korea

The solution for the natural convection in internally finned horizontal annuli is obtained by using a numerical simulation of time-dependent and two-dimensional governing equations. The fins existing in annuli influence the flow pattern, temperature distribution and heat transfer rate. The variations of the fin configuration suppress or accelerate the free convective effects compared to those of the smooth tubes. The effects of fin configuration, number of fins and ratio of annulus gap width to the inner cylinder radius on the fluid flow and heat transfer in annuli are demonstrated by the distribution of the velocity vector, isotherms and streamlines. The governing equations are solved efficiently by using a parallel implementation. The technique is adopted for reduction of the computation cost. The parallelization is performed with the domain decomposition technique and message passing between sub-domains on the basis of the MPI library. The results from parallel computation reveal in consistency with those of the sequential program. Moreover, the speed-up ratio shows linearity with the number of processor.

Key Words : Natural Convection, Finned Annuli, Parallel Computing

1. Introduction

There are many studies for the natural convection in the annuli with constant surface temperatures due to both their theoretical interests and engineering applications such as the storage system of thermal energy, cooling system of electronic and mechanical parts, cooling of electric transmission cable, etc. Kuehn and Goldstein (1970, 1976 and 1978) carried out an experimental and theoretical study for the natural convection in the annulus in concentric and eccentric horizontal cylindrical annuli. They also considered the effects of Prandtl number and diameter ratio on the fluid flow and heat transfer in annuli. After this study, Glakpe et al.(1986), Glakpe and Watkins (1987), Hessami et al. (1984), Ho et al.(1989), Kumar (1987), Mirza and Soliman (1985), Sui and Tremblay (1984), Yang et al.(1988), Yoo (1996) and Van de Sande and Hamer (1979) carried out the experimental and numerical studies to investigate the effects of configuration, boundary conditions, fluid properties and transient responses on the natural convection in the concentric and eccentric annuli. The size and efficiency of this system is determined how much amount of heat is transferred from the inner to outer cylinder, where the main mode of heat transfer is natural convection.

The previous study shows that the heat transfer rate in the horizontal annuli is limited by the surface area of inner cylinder. Thus, the fins are attached on the inner surface of annuli along the longitudinal direction to increase the surface area and heat transfer rate. Chai and Patankar (1993), Desrayaud et al.(2000), Patankar et al. (1979) and Rustum and Soliman (1990) investigated the effects of fins attached on the inner and outer cylinders on the fluid flow and heat transfer

* Corresponding Author,
E-mail : myha@pusan.ac.kr
TEL : +82-51-510-2440; **FAX** : +82-51-512-9835
School of Mechanical Engineering, Pusan National University, San 30, Chang Jeon Dong, Kuem Jeong Gu, Pusan 609-735, Korea. (Manuscript **Received** September 8, 2003; **Revised** January 8, 2004)

in annuli by analyzing the results obtained from the numerical solution of two-dimensional and steady state governing equations. The presence of fins in annuli gives different characteristics of fluid flow and resulting heat transfer, compared to the case without fins. In the present study, we investigate the detail fluid flow and heat transfer characteristics in the presence of fins on the inner cylinder. The effects of fin geometry, number of fins and ratio of the annulus gap to inner radius on the natural convection in annuli are considered. The results with fins are compared with those without fins to see the effects of the presence of fins. The computation is carried out using the parallel computational techniques under MPI (Message Passing Interface).

2. Computational Methodology

The schematic of two-dimensional annuli with fins on the inner surface and the coordinate system is shown in Fig. 1. The system consists of two concentric cylinders with inner and outer radii, R_i and R_o, respectively. The fins, whose height is $L/2$ where $L=R_o-R_i$, are attached on the surface of inner cylinder. The thickness of fins is neglected in the present calculation. The inner cylinder wall is kept at a constant high temperature of T_h, whereas the outer cylinder wall at a constant low temperature of T_c. In this study, we assume that the radiation effects can be taken to be negligible. The fluid properties are also assumed to be constant, except for the density in the buoyancy term, which follows the Boussinesq approximation. The gravitational acceleration acts in the negative y-direction. Thus, in the present study, we observe the fluid flow and thermal fields for the natural convection in annuli with fins on the surface of inner cylinder.

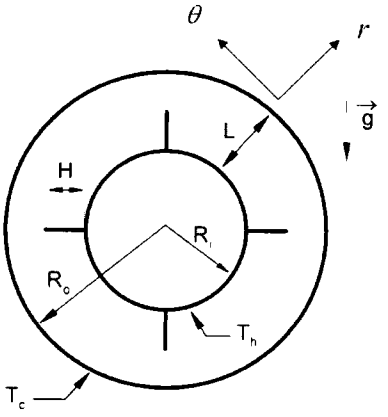

Fig. 1 Schematic of two-dimensional annuli with fins on the inner surface and the coordinate system

We solve the continuity, Navier-Stokes and energy equations in their non-dimensional forms defined as

$$\frac{1}{r}\frac{\partial}{\partial r}(ru_r)+\frac{1}{r}\frac{\partial}{\partial \theta}(u_\theta)=0 \tag{1}$$

$$\begin{aligned}&\frac{\partial u_r}{\partial t}+\frac{\partial}{\partial r}(u_r^2)+\frac{1}{r}\frac{\partial}{\partial \theta}(u_r u_\theta)+\frac{u_r^2-u_\theta^2}{r}\\&=-\frac{\partial p}{\partial r}+Pr\left[\frac{1}{r}\frac{\partial}{\partial r}\left(r\frac{\partial u_r}{\partial r}\right)+\frac{1}{r^2}\frac{\partial^2 u_r}{\partial \theta^2}-\frac{u_r}{r^2}-\frac{2}{r^2}\frac{\partial u_\theta}{\partial \theta}\right]\\&\quad+Pr\Theta Ra\sin\theta\end{aligned} \tag{2}$$

$$\begin{aligned}&\frac{\partial u_\theta}{\partial t}+\frac{\partial}{\partial r}(u_r u_\theta)+\frac{1}{r}\frac{\partial}{\partial \theta}(u_\theta^2)+\frac{2u_r u_\theta}{r}\\&=-\frac{1}{r}\frac{\partial p}{\partial \theta}+Pr\left[\frac{1}{r}\frac{\partial}{\partial r}\left(r\frac{\partial u_\theta}{\partial r}\right)+\frac{1}{r^2}\frac{\partial^2 u_\theta}{\partial \theta^2}-\frac{u_\theta}{r^2}-\frac{2}{r^2}\frac{\partial u_r}{\partial \theta}\right]\\&\quad+Pr\Theta Ra\cos\theta\end{aligned} \tag{3}$$

$$\begin{aligned}&\frac{\partial \Theta}{\partial t}+\frac{\partial}{\partial r}(u_r\Theta)+\frac{1}{r}\frac{\partial}{\partial \theta}(u_\theta\Theta)\\&=\frac{1}{r}\frac{\partial}{\partial r}\left(r\frac{\partial \Theta}{\partial r}\right)+\frac{1}{r^2}\frac{\partial^2\Theta}{\partial \theta^2}\end{aligned} \tag{4}$$

The dimensionless variables in the above equations are defined as

$$\begin{aligned}&t=\frac{t^*\alpha}{L^2},\ r=\frac{r^*}{L},\ u_r=\frac{u_r^*L}{\alpha},\ u_\theta=\frac{u_\theta^*L}{\alpha},\\&P=\frac{P^*L^2}{\rho\alpha^2},\ \Theta=\frac{T-T_c}{T_h-T_c}\end{aligned} \tag{5}$$

In the above equations, ρ, T and α represent the density, dimensional temperature and thermal diffusivity. The superscript $*$ in equation (4) represents the dimensional variables. u_r, u_θ, p, Θ, t, r and θ are the non-dimensional radial velocity, circumferential velocity, pressure, temperature, time, radial coordinate and circumferential coordinate. The above non-dimensionalization results in two dimensionless parameters:

$Pr=\frac{\nu}{\alpha}$ and $Ra=\frac{g\beta L^3(T_h-T_c)}{\nu\alpha}$ where ν, g and β are the kinematic viscosity, gravitational acceleration and volume expansion coefficient. In the simulations to be reported here the Prandtl number, Pr, has been taken to be 0.7 corresponding to that of air. The Rayleigh number, Ra, varies in the range of $10^3 \sim 10^6$.

A spectral multi-domain methodology is used to consider the fins attached on the surface of inner cylinder. The spatial discretization in radial (r) and circumferential (θ) directions is performed using a spectral multi-domain technique. In this technique, the overall computational domain is subdivided into a number of smaller sub-domains. Within each sub-domain, a local spectral Chebyshev discretization is defined. The discrete approximation of derivatives at each point in a domain utilizes only points within the same domain. The detail explanation for the a spectral multi-domain technology is given in Parker (2002). Figure 2 shows the computational geometry involving 6 subdomains in the $r-\theta$ plane, with each subdomain resolved up to 16×30 points. A two-step time-split scheme is used to advance the flow field. First the velocity is advanced from time level 'n' to an intermediate level by solving the advection-diffusion equation. In the advection-diffusion step, the nonlinear terms are treated explicitly using third-order Adams-Bashforth scheme. The diffusion terms are treated implicitly using Crank-Nicholson scheme. Then a Poisson equation for pressure is solved fully implicitly. The final divergence-free velocity field at 'n+1' is obtained with a pressure-correction step. After obtaining the velocity field, the temperature field is advanced in a similar manner with third-order Adams-Bashforth for the advection term and Crank-Nicholson scheme for the diffusion term. Once the velocity and temperature fields are obtained, the local, surface-averaged, and time- and surface-averaged Nusselt number at the inner and outer cylinder walls are defined as

$$Nu=\frac{dD_h}{k_f}=\frac{\partial\Theta}{\partial n}\Big|_{wall}$$
$$\overline{Nu}=\frac{1}{2\pi}\int_0^{2\pi}Nu\,d\theta \quad <\overline{Nu}>=\frac{1}{t_p}\int_0^t \overline{Nu}\,dt \tag{6}$$

where h, D_h, k, n and t_P are the heat transfer coefficient, hydraulic diameter, thermal conductivity, normal direction to walls and time integration period, respectively. All time-averages to be reported here are obtained by averaging only over the stationary state (the initial transient phase is ignored). For the velocity field, the no-slip and no-penetration boundary conditions are imposed on the walls. The cold wall temperatures of $\Theta=0$ is imposed on the outer cylinder wall, whereas the hot wall temperatures of $\Theta=1$ on the inner cylinder wall and fins.

The developed computer code is parallelized based on the MPI (Message Passing Interface) to increase the computational speed. Table 1 shows the specification of the computer hardware and MPI libraries used for the parallelization of the developed code. We used the virtual topology method in the MPI programming technique. In the virtual topology method, the processors

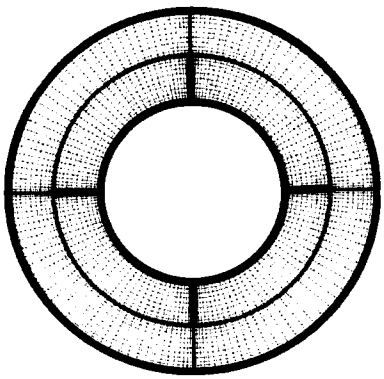

Fig. 2 Computational geometry and mesh used

Table 1 Specification of PC Cluster used

Hardware	CPU	Dual Intel Pentium III 550 MHz
	Memory	512 Mbytes SDRAM
	LAN-Card	Universal, 64/32-bit, 66/33 MHz, Myrinet-LAN
	Switch	16-port Myrinet-LAN switch
software	OS	Alzza linux 6.1, MPICH-1.2.1
	Parallel Application	MPICH-1.2.1

used in the parallel computation are arranged virtually in two- or three-dimensional way and have their own independent coordinates. Using this method, we can make the programming for the data exchange between the processors during the parallel computing easier and manage flexibly the change in the number of processors used in the parallel computing. The two-dimensional virtual topology method is used in the present study. The number of processors used is 12 in the streamwise direction and 2 in the cross-streamwise direction, respectively. The same number of grid points is allocated to each processor. In order to perform the fast and highly efficient calculation in the parallel computation, the computation time allocated to each processor is equally distributed and the boundary values between the adjacent processors should be treated very carefully. The direct solver is used in the present calculation to obtain the solution for the discretized algebraic equations. We also used the influence matrix method to exchange the computed results at the interface between the adjacent processors and to obtain the continuous values for the dependent variables of velocities, pressure and temperature at the interface. The computation time is decreased almost linearly to the number of processors used in the present calculation.

3. Results and Discussion

For the purpose of code validation, the natural convection problem in annuli without fins was tested for different values of Rayleigh number and ratio of the annulus gap to inner radius ($\sigma=L/R_i$). Table 2 shows the surface-averaged Nusselt numbers at the inner and outer cylinder walls, $\overline{Nu_i}$ and $\overline{Nu_o}$ for different σ values when $Ra=10^4$. The surface-averaged Nusselt number, $\overline{Nu}$, in Table 2 is defined by normalizing its value using conduction-limited Nusselt number, $\overline{Nu_c}$. The present computational results are compared with the experimental ones obtained by Kuehn and Goldstein (1976) and the computational ones by Yoo (1996). Figure 3 shows the comparison of present results for the local Nusselt numbers at the inner and outer cylinder walls as a function of θ with experimental results given by Kuehn and Goldstein (1976) when $\sigma=0.625$ and $Ra=4.7\times10^4$. Figure 4 shows the comparison of present results for the local Nusselt numbers at the inner and outer cylinder walls as a function of θ with computational results given by Yoo (1996) when

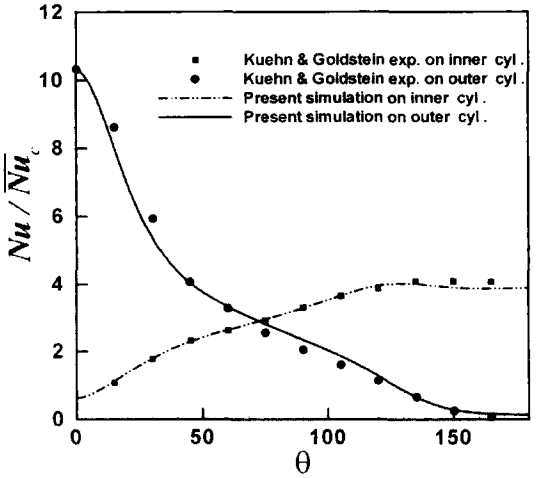

Fig. 3 Comparison of the local Nusselt number at the inner and outer cylinder walls as a function of θ with experimental results when $\sigma=0.625$ and $Ra=4.7\times10^4$

Table 2 Surface-averaged Nusselt number at the inner and outer cylinder wall for different σ values when $Ra=10^4$

σ	Present	Goldstein (1976)	Yoo (1996)
	$(\overline{Nu_i}/\overline{Nu_c}, \overline{Nu_o}/\overline{Nu_c})$	$(\overline{Nu_i}/\overline{Nu_c}, \overline{Nu_o}/\overline{Nu_c})$	$(\overline{Nu_i}/\overline{Nu_c}, \overline{Nu_o}/\overline{Nu_c})$
0.25	(2.110, 2.076)	(2.148, 2.157)	(2.082, 2.109)
0.5	(2.044, 2.004)	(2.061, 2.059)	(2.022, 2.037)
0.625	(1.994, 1.952)	(2.010, 2.005)	(1.973, 1.985)
1.0	(1.857, 1.811)	(1.850, 1.853)	(1.837, 1.848)

σ=0.625 and Ra=4×10³. The streamlines and isotherms obtained from the present computation are also compared with those by Yoo (1996), giving excellent agreement between them. All these comparisons show that the present computational results for the natural convection in annuli without fins represent well the experiment results obtained by Kuehn and Goldstein (1976) and the computational results by Yoo (1996), showing the excellent agreement among them.

Figure 5 shows the schematic for different fin arrangements of '+' and 'x'-shapes in annuli to investigate the effects of fin arrangement on the fluid flow and temperature distribution in the enclosure when σ=1 and Ra=10⁴~10⁶. Figure 6 shows the streamlines and isotherms for the different fin arrangement at the Rayleigh numbers of 10⁴, 10⁵ and 10⁶. When Ra=10⁴ and the fins have a '+'-shape, the fluid (air) at the lower part is heated by heat transfer from the hot inner cylinder and the bottom fin and moves upwards along the surface of inner cylinder. If the fluid meets the second fin located at the center of the annuli, the fluid is forced to bend and moves along the fin. The fluid at the upper part keeps moving upward along the surface of inner cylinder and top fin due to the continuous heating by heat transfer from the second and third fins and the inner hot cylinder. If the ascending flow meets the cold outer cylinder, it changes its direction and moves downwards along the outer cold wall. Due to the presence of fins, we can observe two almost closed circulating bubbles, compared

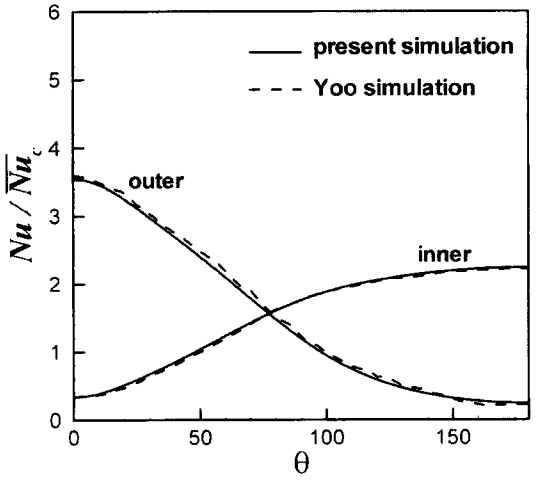

Fig. 4 Comparison of the local Nusselt number at the inner and outer cylinder walls as a function of θ with Yoo's calculation results when σ=0.625 and Ra=4×10³

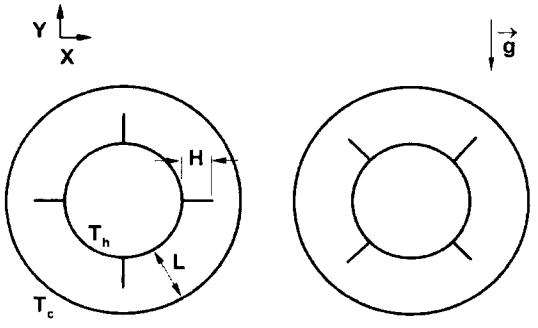

Fig. 5 Schematic for different fin arrangements of '+' and "x"-shapes in annuli

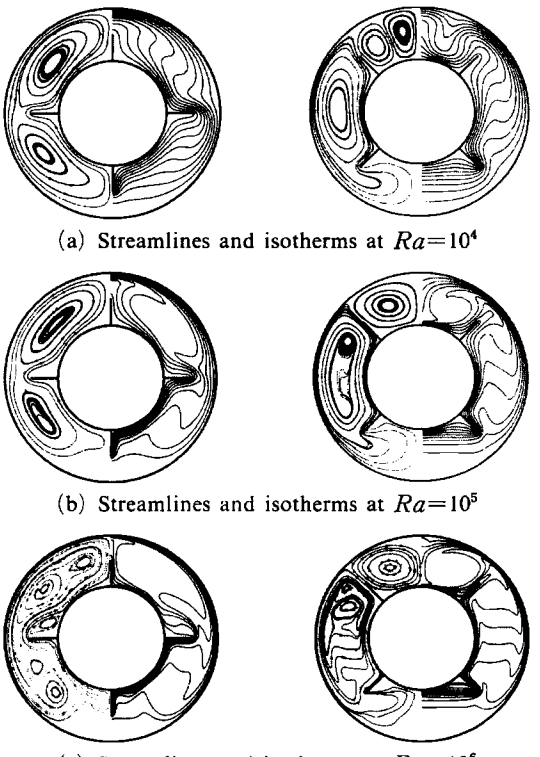

(a) Streamlines and isotherms at Ra=10⁴

(b) Streamlines and isotherms at Ra=10⁵

(c) Streamlines and isotherms at Ra=10⁶

Fig. 6 Streamlines and isotherms for different fin arrangement at the Rayleigh number of 10⁴, 10⁵ and 10⁶

to a single bubble for the case of the natural convection in annuli without fins at $Ra=10^4$. The distribution of isotherms generally follows the flow fields. The isotherms rotate in the clockwise and counterclockwise directions in the right and left sides of the enclosure, respectively. When $Ra=10^4$ and the fins have a 'x'-shape, the distribution of streamlines and isotherms is different form that with '+'-shaped fins. At the bottom part of the enclosure, the outer cylinder at a constant low temperature is located at the lower part relatively in the vertical (gravity) direction than the inner cylinder at a constant high temperature. Thus the fluid in between the inner and outer cylinders at the lower part is in a stable condition and is almost stagnant. The mode of heat transfer is conduction and the isotherms are almost parallel to the horizontal direction. The fluid in between the first and second fin for the case of 'x'-shaped fins is heated by heat transfer from the hot inner cylinder and fins, and moves upwards along the surface of inner cylinder, similar to the flow for the case of '+'-shaped fins. If the ascending fluid along the inner cylinder meets the second fin at the upper part, the flow keeps moving upwards along the lower part of the second fin, changes its direction after it meets the cold outer cylinder, moves downwards along the outer cold wall, and forms closed large vortices. Thus the isotherms in between the first and second fin for the case of 'x'-shaped fins also follows the flow and have the similar shape to that of '+'-shaped fins. At the top part of enclosure, the outer cylinder at a constant low temperature is located at the upper part relatively in the vertical (gravity) direction than the inner cylinder at a constant high temperature, which is opposite to the bottom part of enclosure. Thus the fluid in between fins at the top part is in an unstable condition and shows the pattern similar to the fluid flow and heat transfer for the case of Rayleigh-Benard convection in the horizontal rectangular enclosure. The fluid flow forms two pairs of roll cells circulating in the clockwise and counterclockwise direction and isotherms have a mushroom shape at the top part of enclosure. From these results, we can deduce that the streamlines and isotherms in the annuli with '+'-shaped fins have generally the similar characteristic to those in the vertical rectangular enclosure. However, the characteristics of streamlines and isotherms in the annuli with 'x'-shaped fins are divided into three regions. At the bottom region of enclosure, the distribution of streamlines and isotherms is similar to that for the case of horizontal rectangular enclosure with a lower plate at the low temperature and an upper plate at the high temperature. The shapes of streamlines and isotherms in the region between the first and second fin are similar to those for the case of vertical rectangular enclosure. At the top region of enclosure, the pattern of streamlines and isotherms is similar to that for the case of horizontal rectangular enclosure with a lower plate at the high temperature and an upper plate at the low temperature.

When the Rayleigh number is increased to 10^5 and the fins have a '+'-shape, the pattern of streamlines and isotherms is generally similar to that at $Ra=10^4$, as shown in Fig. 6(b). However, with increasing Rayleigh number, we can observe the development of boundary layers along the surfaces of inner and outer cylinders due to increasing heat transfer. The magnitude of velocity increases, thermal gradients at the hot inner and cold outer cylinders increase, and the core region in between the inner and outer cylinder is well mixed with decreasing thermal gradient. When $Ra=10^5$ and the fins have a 'x'-shape, the shape of streamlines and isotherms at the bottom and in between the first and second fins of annuli is also similar to that for $Ra=10^4$. However, the pattern of streamlines and isotherms at the top region of annuli for $Ra=10^5$ is different from that for $Ra=10^4$. With increasing Rayleigh number, the size of roll cell becomes wider in the circumferential direction since the number of roll cells in the circumferential direction suffers a quantum jump from two pairs of rolls at $Ra=10^4$ to one pair at $Ra=10^5$. Corresponding change can be seen in the isotherms also well.

For $Ra \leq 10^5$, the flow is steady and correspondingly isotherms and streamlines are time-

invariant for both cases with '+' and 'x'-shaped fins in the annuli. However, when $Ra=10^6$ and the fins have a '+'-shape, the fluid flow and temperature fields in the annuli become time-dependent like the case for the annuli without internal fins at the same Rayleigh number. Thus the isotherms and streamlines in Figure 6(c) show the time-averaged temperature and velocity fields. With increasing Rayleigh number, we can observe the secondary and tertiary flows in the annuli with larger temperature gradients near the inner and outer cylinder surfaces and lower temperature gradients in the core region in between the inner and outer cylinders. However, when $Ra=10^6$ and the fins have a 'x'-shape, the fluid flow and temperature fields in the annuli are still time-invariant like both cases of '+' and 'x'-shaped fins at $Ra\leq 10^5$ and unlike the case of '+'-shaped fin at $Ra=10^6$. The shapes of fluid flow and temperature fields at the bottom, middle and top parts in the annuli are divided into three different regimes of conduction in the horizontal enclosure, natural convection in the vertical enclosure and natural convection in the horizontal enclosure, due to the presence of 'x'-shaped fins. At the middle part between the first and second fins of annuli, we can observe the development of thin boundary layer, strong temperature gradients along the cylinder surfaces and an almost uniform temperature gradient along the circumferential direction in the interior region. At the top part of annuli, the shapes of streamlines and isotherms at $Ra=10^6$ are similar to those at $Ra=10^5$ with a pair of roll cell vortices and mushroom-shaped isotherms. However, with increasing Rayleigh number, the magnitude of velocity become larger, resulting in the larger thermal gradient at the walls and smaller gradient in the core region.

Figure 7(a) shows local Nusselt number distribution along the surfaces of inner cylinder with '+'-shaped fins for different Rayleigh numbers of 10^4 and 10^5. The local Nusselt number is normalized by the average Nusselt number for conduction between two cylinders. The local Nusselt number has the highest value at the tip of bottom fin, because the cold fluid impinges on the hot fin at the bottom. This is confirmed by the densely packed isotherms around bottom fin tip, as shown in Figure 5. When fluid moves toward the fin base from the tip, flow loses momentum due to the wall resistance. Thus in the regions near the fin bases the fluid is actually stagnant and the fluid temperature is almost close to the wall temperature of fin and inner cylinder, resulting in a near-zero local Nusselt number. When we move away from the fin bases at the middle and top parts, it gains momentum, resulting in the increase in the velocity and local Nusselt number (heat transfer) and reaching a maximum value at the tip. When the fluid moves away from the fin base along the inner cylinder,

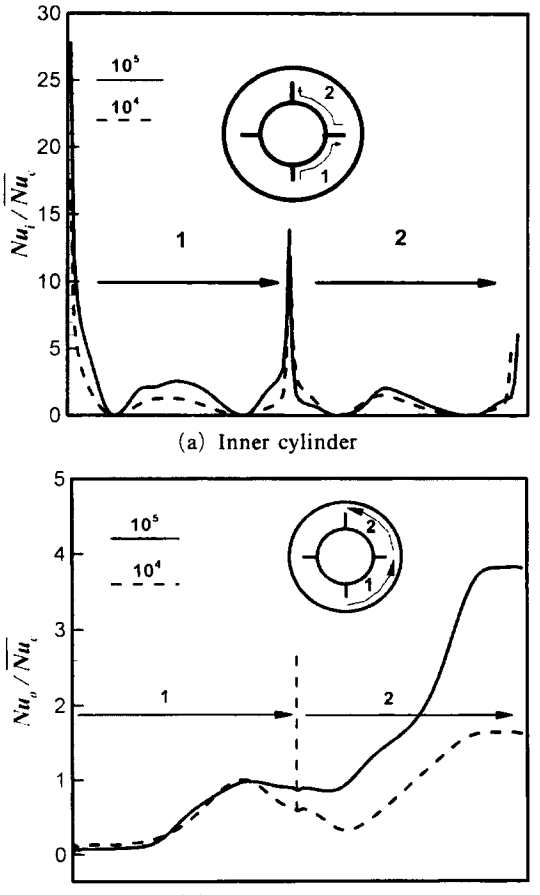

(a) Inner cylinder

(b) Outer cylinder

Fig. 7 Local Nusselt number distribution along the surfaces of inner and outer cylinder with '+'-shaped fins for different Rayleigh number of 10^4 and 10^5

the local Nusselt number increases due to the flow impingement on the inner cylinder and the momentum gain. However, when the fluid moves toward the next fin base along the inner cylinder the local Nusselt number decreases again due to the above-mentioned reason. Figure 7(b) shows local Nusselt number distribution along the surfaces of outer cylinder with '+'-shaped fins for different Rayleigh numbers of 10^4 and 10^5. At the top of outer cylinder, the local Nusselt number has the highest value due to the impingement of downward flow on the outer cylinder. When fluid moves downwards along the outer cylinder from the top in the bay 2 the local Nusselt number decreases due to the development of thermal boundary layer. At the location close to the middle fin, the local Nusselt number increases slightly due to another flow impingement on the outer cylinder caused by the recirculating flow in the bay 1. When we move downwards along the outer cylinder in the bay 1, the local Nusselt number keeps decreasing with the development of thermal boundary layer and reaches almost the constant minimum value. As expected, the local Nusselt number increases with increasing Rayleigh number due to increasing velocity.

Figure 8(a) shows local Nusselt number distribution along the surfaces of inner cylinder with 'x'-shaped fins for different Rayleigh numbers of 10^4 and 10^5. The shape of local Nusselt number distribution along the surface of inner cylinder for the case with 'x'-shaped fins is generally similar to that with '+'-shaped fins. The local Nusselt number has the highest peak values at the fin tips and near-zero values around the fin bases. The local Nusselt number decreases with the momentum gain as fluid moves away from the fin bases, whereas it decreases with the momentum loss due to the wall friction as fluid moves towards the fin bases. Figure 8(b) shows local Nusselt number distribution along the surfaces of outer cylinder with 'x'-shaped fins for different Rayleigh numbers of 10^4 and 10^5. The local Nusselt number at the outer cylinder has the highest value around the top due to the impingement of hot fluid on the outer cylinder. The local Nusselt number for 'x'-shaped fins decreases along the surface of outer cylinder when we move downwards along the outer cylinder from the top fin to the bottom of annuli, similar to that for '+'-shaped fins. However, when $Ra=10^4$, two pairs of vortices are formed at the top part of annuli. Due to the presence of two pairs of vortices, when we move from the top fin to the top part of annuli, the local Nusselt number keeps decreasing until it reaches the lower peak value at the location of downwelling plume and then increases again. The number of roll cells at the top part suffers a quantum jump from two pairs of rolls at $Ra=10^4$ to one pair at $Ra=10^5$. Thus

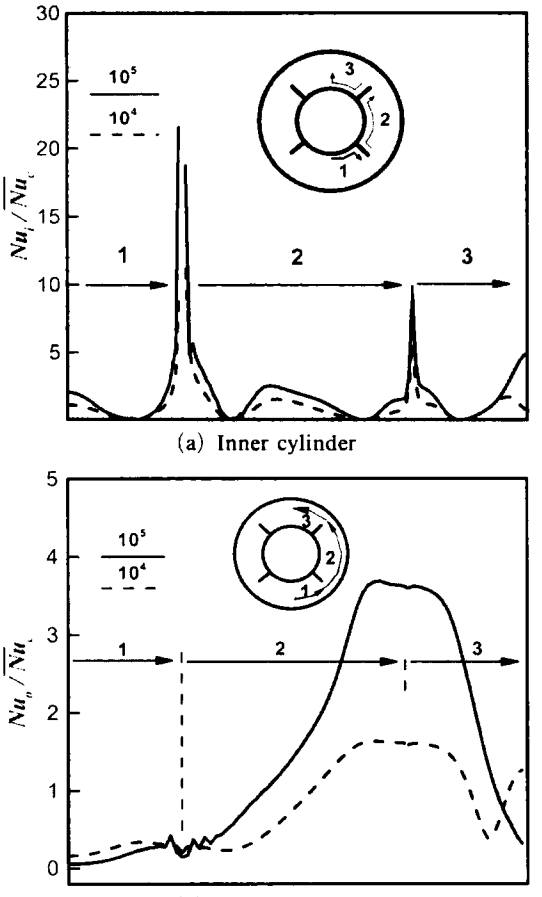

Fig. 8 Local Nusselt number distribution along the surfaces of inner and outercylinder with 'x' shaped fins for different Rayleigh number of 10^4 and 10^5

the local Nusselt number at $Ra=10^5$ keeps decreasing as fluid moves from the fin tip to the top part of annuli, unlike to the case of $Ra=10^4$.

Figure 9 shows the time history of surface-averaged Nusselt number at the inner cylinder for different cases with and without fins at $Ra=10^6$. For the case of 'x'-shaped fins, the fluid flow and temperature fields in the annuli are time-independent as shown in Figure 6, giving the steady surface-averaged Nusselt number. However, for the cases without fins and with '+'-shaped fins, the surface-averaged Nusselt number becomes time-dependent with time-varying fluid flow and temperature fields. The surface-averaged Nusselt number for the case without fins is regularly repeated in a periodic fashion with a period of 0.005 dimensionless times. However, the local Nusselt number for the case with 'x'-shaped fins oscillates in a chaotic pattern with higher amplitude compared to the case without fins. Table 3 shows the surface- and time-averaged Nusselt numbers, $\langle\overline{Nu_i}\rangle$, at the inner cylinder wall for different Rayleigh numbers when $\sigma=2$. The present computational results for '+'- and 'x'-shaped fins are compared with those without fins. The values of Nusselt number for the cases with fins are less than those without fins, due to the flow resistance in the presence of fins. The Nusselt number for the case with 'x'-shaped fins is slightly larger than that with '+'-shaped fins, due to more active mixing on the top part for the case of 'x'-shaped fins compared to the case of '+'-shaped fins.

Figures 10 shows the velocity vectors and isotherms for the different fin numbers of $N=4$,

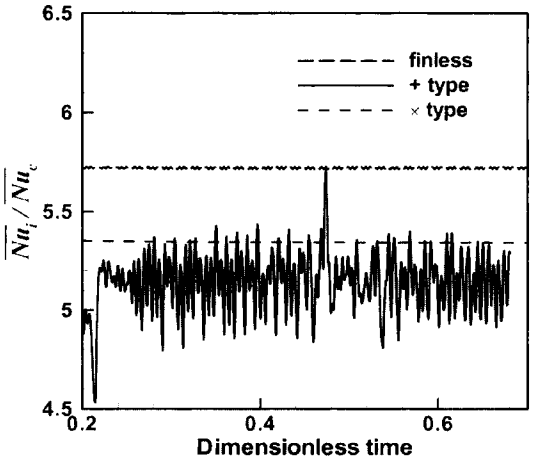

Fig. 9 Time history of surface-averaged Nusselt number at the inner cylinder for different cases with and without fins at $Ra=10^6$

Table 3 Surface- and time-averaged Nusselt number at inner cylinder wall for different Rayleigh number when $\sigma=2$

	+-type	X-type	finless
	$(\overline{Nu_i}/\overline{Nu_c})$	$(\overline{Nu_i}/\overline{Nu_c})$	$(\overline{Nu_i}/\overline{Nu_c})$
10^4	1.6822	1.7280	1.8332
10^5	2.9121	3.1033	3.3305
10^6	5.1824	5.3418	5.7210

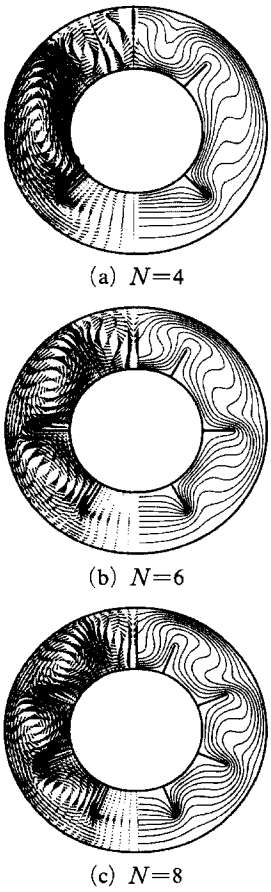

(a) $N=4$

(b) $N=6$

(c) $N=8$

Fig. 10 Velocity vectors and isotherms for the different fin numbers of $N=4$, 6 and 8 when $Ra=10^4$ and $\sigma=2$

6 and 8 when $Ra=10^4$ and $\sigma=2$. When $Ra=10^4$, the characteristics of streamlines and isotherms in the annuli for $N=6$ and 8 show three different patterns, similar to those for $N=4$ corresponding to the case of 'x'-shaped fins in Figures 6(a) and 10(a). The distribution of velocity vectors and isotherms at the bottom part is similar to the fluid flow and heat transfer for the case of stable horizontal rectangular enclosure with a lower plate at the low temperature and an upper plate at the high temperature, whereas velocity vectors and isotherms at the top part have a similar pattern to the case of unstable horizontal rectangular enclosure with a lower plate at the high temperature and an upper plate at the low temperature. The shapes of streamlines and isotherms formed in the regions between the first fin at the lower part and last fin at the upper parts are similar to those for the case of inclined vertical rectangular enclosure. We can observe a closed single cell in each bay between the first fin at the lower part and last fin at the upper parts. A striking difference observed at the top bay in between fins located at the upper part is a quantum jump in the number of roll cells from two pairs when $N=4$ to one pair when $N=6$ and 8 because the size of top bay decreases with increasing number of fins. When the Rayleigh number is increased to 10^5, the general pattern of velocity vectors and isotherms is similar to the case for $Ra=10^4$, showing three different shapes of fluid flow and heat transfer observed in the stable and unstable horizontal enclosures and the inclined vertical enclosure, as shown in Figure 11. Due to increasing magnitude of velocity with increasing Rayleigh number, thermal gradients at the hot inner and cold outer cylinders increase, and the core region enclosed by the fins and cylinders is well mixed with decreasing thermal gradient. The main differences are that the number of roll cells formed at the top bay of annuli is a single pair for all the cases of $N=4$ when $Ra=10^5$, unlike to two pairs of roll cells for $N=4$ when $Ra=10^4$, because the size of roll cells becomes wider with increasing velocity. The

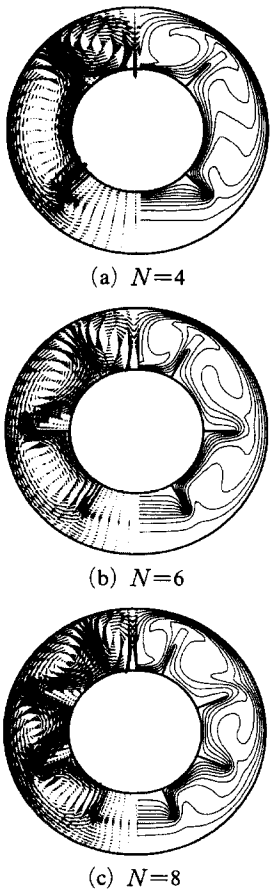

Fig. 11 Velocity vectors and isotherms for the different fin numbers of $N=4$, 6 and 8 when $Ra=10^5$ and $\sigma=2$

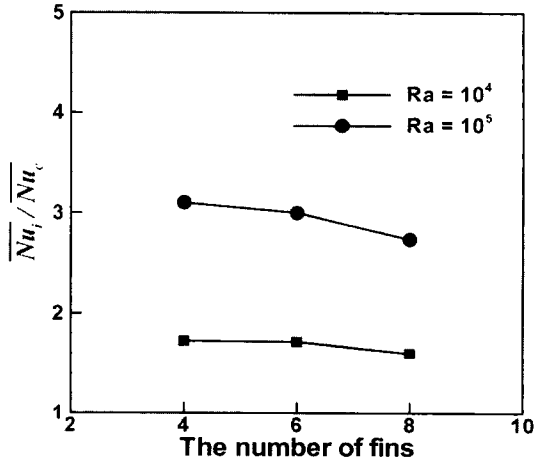

Fig. 12 Surface-averaged Nusselt number at the inner cylinder for different number of fins at $Ra=10^4$ and 10^5

number of roll cell for $N=6$ and 8 at $Ra=10^5$ is one, which is the same as the case at $Ra=10^4$. We can also observe secondary corner vortices formed around the base of fins at $Ra=10^5$, unlike a single vortex formed in each bay between the first fin at the lower part and last fin at the upper parts at $Ra=10^4$.

Figure 12 shows the surface-averaged Nusselt number, $\overline{Nu_i}$, at the inner cylinder for different number of fins at $Ra=10^4$ and 10^5. $\overline{Nu_i}$ decreases slightly due to increasing flow resistance with increasing number of fins. $\overline{Nu_i}$ at $Ra=10^5$ is larger than that at $Ra=10^4$, due to increasing velocity with increasing Rayleigh number.

Figure 13 shows the velocity vectors and isotherms for the different values of $\sigma=1\sim4$ at $Ra=10^5$. The size of annulus gap decreases with increasing σ, resulting in increasing aspect ratio in each bay. The velocity vectors and isotherms have generally similar patterns for different values of σ, which show the fluid flow and heat transfer characteristics corresponding to the stable and unstable horizontal enclosures and inclined vertical enclosure as stated above. The striking differences observed by increasing the value of σ are the number of roll cells formed on the top bay. When $\sigma=1$ and 2, we can observe a pair of roll cells formed on the top bay. When σ is increased to 3, the secondary vortices are formed close to the main vortices. The size of secondary vortices is small compared to the main vortices, When $\sigma=4$, the size of secondary vortices increases to that of main vortices, forming two pairs of roll cells on the top bay. In the inclined vertical enclosure, we can observe closed main vortices formed in each bay with very small corner vortices. The size of corner vortices in the inclined vertical enclosure increases when we move from the bottom to top bay. The magnitude of velocity at the bottom bay is very small.

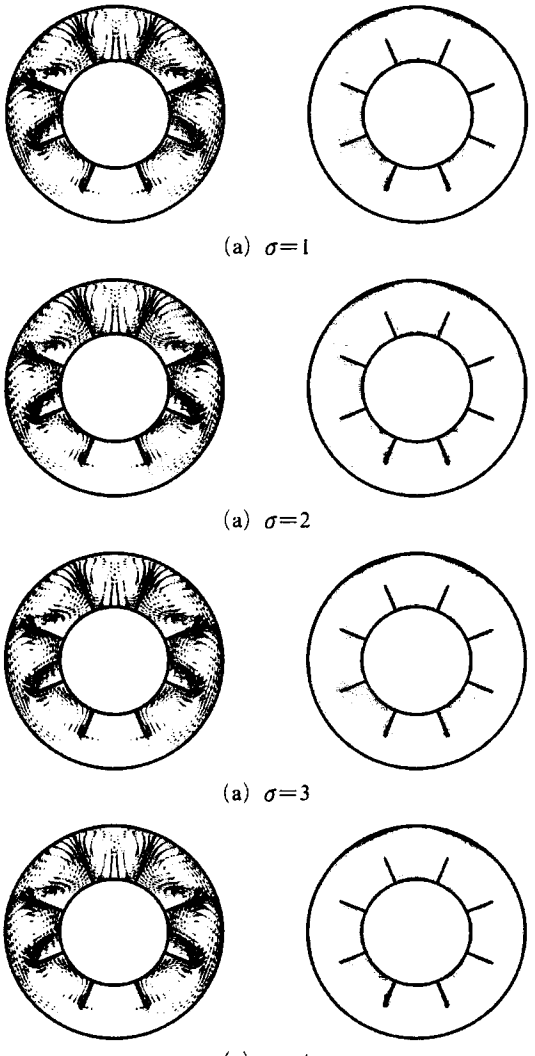

Fig. 13 Velocity vectors and isotherms for the different values of $\sigma=1\sim4$ at $Ra=10^5$

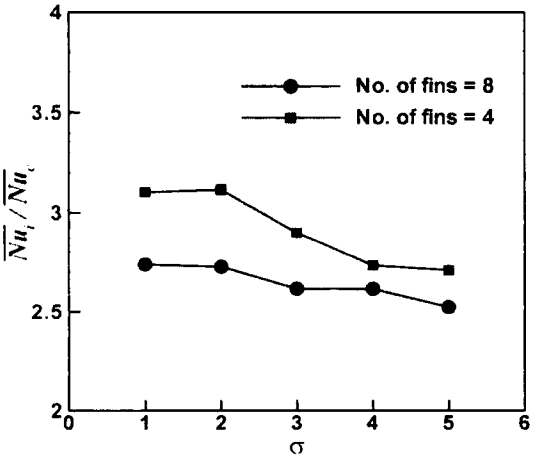

Fig. 14 Surface-averaged Nusselt number at the inner cylinder as a function of σ for different number of fins at $Ra=10^5$

Figure 14 shows the surface-averaged Nusselt number, $\overline{Nu_i}$, at the inner cylinder as a function of σ for different number of fins at $Ra=10^5$. With increasing σ, the size of annulus gap decreases and the flow resistance increases, resulting in decreasing $\overline{Nu_i}$. $\overline{Nu_i}$ for the number of fins of $N=8$ is larger than that for $N=4$, as explained previously.

4. Conclusions

We solved the unsteady natural convection problem in annuli with fins attached on the inner cylinders using an accurate and efficient Chebyshev spectral collocation approach and parallel computing implementation. A multi-domain methodology is used to address the geometric complexity posed by the fins. The results for the case with internal fins are compared with those without internal fins, to see the effects of the presence of fins.

The configuration of internal fins gives different fluid flow and heat transfer in annuli. When the fins have a '+'-shape, the fluid flow and heat transfer in between fins are similar to those in the vertical rectangular enclosure. However, the natural convection in the annuli with 'x'-shaped fins are generally divided into three regions corresponding to the fluid flow and heat transfer in the stable and unstable horizontal rectangular enclosures and in the inclined vertical rectangular enclosure. The values of Nusselt number with 'x'-shaped fins are slightly larger than those with '+'-shaped fins. The Nusselt number decreases with increasing number of fins and ratio of the annulus gap to inner radius and increases with increasing Rayleigh numbers.

Acknowledgment

This work was partially supported by the BK21 and NRL projects.

References

Chai, J. C. and Patankar, S. V., 1993, "Laminar Natural Convection in Internally Finned Horizontal Annuli," *Numerical Heat Transfer, Part A*, Vol. 24, pp. 67~87.

Desrayaud, G., Lauriat, G. and Cadiou, P., 2000, "Thermoconvective Instabilities in a Narrow Horizontal Air-filled Annulus," *Int. J. Heat Fluid Flow*, Vol. 21, pp. 65~73.

Farinas, M., Garon, A. and Saint-Louis, K., 1997, "Study of Heat Transfer in a Horizontal Cylinder with Fins," *Rev Cen Therm*, Vol. 36, pp. 398~410.

Glakpe, E. K., Watkins, Jr., C. B. and Cannon, J. N., 1986, "Constant Heat Flux Solutions for Natural Convection between Concentric and Eccentric Horizontal Cylinders," *Numer. Heat Transfer*, Vol. 10, pp. 279~295.

Glakpe, E. K. and Watkins, Jr., C. B., 1987, "Effect of Mixed Boundary Conditions on Natural Convection in Concentric and Eccentric Annular Enclosure," *AIAA Paper*, pp. 1587~1591.

Hessami, M. A., Pollard, A. and Rowe, R. D., 1984, "Numerical Calculations of Natural Convection Heat Transfer between Horizontal Concentric Isothermal Cylinders - Effects of Variation of Fluid Properties," *J. Heat Transfer*, Vol. 106, pp. 668~671.

Ho, C. J., Lin, Y. H. and Chen, T. C., 1989, "A Numerical Study of Natural Convection in Concentric and Eccentric Horizontal Cylindrical Annuli with Mixed Boundary Conditions," *Int. J. Heat Fluid Flow*, Vol. 10, pp. 40~47.

Kuehn, T. H. and Goldstein, R. J., 1970, "A Parametric Study of Prandtl Number and Diameter Ratio Effects on Natural Convection Heat Transfer in Horizontal Cylindrical Annulus," *J. Heat Transfer*, Vol. 102, pp. 768~770.

Kuehn, T. H. and Goldstein, R. J., 1976, "An Experimental and Theoretical Study of Natural Convection in the Annulus between Horizontal Concentric Cylinders," *J. Fluid Mech.*, Vol. 74, pp. 695~719.

Kuehn, T. H. and Goldstein, R. J., 1978, "An Experimental Study of Natural Convection Heat Transfer in Concentric and Eccentric Horizontal Cylindrical Annuli," *J. Heat Treansfer*, Vol. 100, pp. 635~640.

Kumar, R., 1987, "Numerical Study of Natural

Convection in a Horizontal Annulus with Constant Heat Flux on the Inner Wall," *Proceedings of the 1987 ASME-JSME Thermal Engineering Joint Conference*, Vol. 2, pp. 187~193.

Mirza, S. and Soliman, H. M., 1985, "The Influence of Internal Fins on Mixed Convection inside Horizontal Tubes," *Int. Commun. Heat Mass Transfer*, Vol. 12, pp. 191~200.

Parker, S. J., 2002, "Stability and Vortex Shedding of Bluff Body Arrays," PhD Thesis, University of Illinois, Urbana, IL.

Patankar, S. V., Ivanovic, M. and Sparrow, E. M., 1979, "Analysis of Turbulent Flow and Heat Transfer in Internally Finned Tubes and Annuli," *J. Heat Transfer*, Vol. 101, pp. 29~37.

Rustum, I. M. and Soliman, H. M., 1990, "Numerical Analysis of Laminar Mixed Convection in Horizontal Internally Finned Tubes," *Int. J. Heat Mass Transfer*, Vol. 33., pp. 1485~1496.

Sui, Y. T. and Tremblay, B., 1984, "On transient Natural Convection Heat Transfer in the Annulus between Concentric Horizontal Cylinders with Isothermal Surfaces," *Int. J. Heat Mass Transfer*, Vol. 27, pp. 103~111.

Van de Sande, E. and Hamer, B. J. G., 1979, "Steady and Transient Natural Convection in Enclosures between Circular Cylinders (Constant Heat Flux)," *Int. J. Heat Mass Transfer*, Vol. 22, pp. 361~370.

Yang, H. Q., Yang, K. T. and Lloyd, J. R., 1988, "Natural Convection Suppression in Horizontal Annuli by Azimuthal Baffles," *Int. J. Heat Mass Transfer*, Vol. 31, pp. 2123~2136.

Yoo, J., 1996, "Dual Steady Solutions in Natural Convection Between Horizontal Concentric Cylinders," *Int. J. Heat Fluid Flow*, Vol. 17, pp. 587~593.